International Journal of Mechanical Sciences 89 (2014) 350–361

Contents lists available at ScienceDirect

International Journal of Mechanical Sciences

journal homepage: www.elsevier.com/locate/ijmecsci

Acoustic metamaterial plates for elastic wave absorption and structural vibration suppression

Hao Peng *, P. Frank Pai

Department of Mechanical and Aerospace Engineering, University of Missouri, Columbia, MO 65211, USA

ARTICLE INFO

Article history:
Received 7 February 2014
Received in revised form
2 September 2014
Accepted 29 September 2014
Available online 7 October 2014

Keywords:
Acoustic metamaterial plate
Vibration absorber
Stopband
Dispersion
Negative effective mass
Elastic wave propagation

ABSTRACT

This article presents the design and modeling techniques and design guidelines, and reveals the actual working mechanism of acoustic metamaterial plates for elastic wave absorption and structural vibration suppression. Each of the studied metamaterial plates is designed by integrating two (or one) isotropic plates with distributed discrete mass-spring-damper subsystems that act as local vibration absorbers. For an infinite metamaterial plate, its stopband is obtained by dispersion analysis on an analytical unit cell. For a finite metamaterial plate with specific boundary conditions, frequency response analysis of its full-size finite-element model is performed to show its stopband behavior, and the stopband behavior is further confirmed by transient analysis based on direct numerical integration of the finite-element equations. Influences of the vibration absorbers' local resonant frequencies and damping ratios and the plate's damping, boundary conditions, and natural frequencies and mode shapes are thoroughly examined. The concepts of negative effective mass and spring and acoustic and optical wave modes are explained in detail. The working mechanism of acoustic metamaterial plates is revealed to be based on the concept of conventional vibration absorbers. An absorber's resonant vibration excited by the incoming elastic wave generates a concentrated inertial force to work against the plate's internal shear force, straighten the plate, and attenuate/stop the wave propagation. Numerical results show that the stopband's location is determined by the local resonant frequency of absorbers, the stopband's width increases with the (absorber mass)/(unit cell mass) ratio, and increase of absorbers' damping significantly increases the stopband's width and reduces low-frequency vibration amplitudes. However, too much damping may deactivate the stopband effect, and the plate's material damping is not as efficient as absorbers' damping for suppression of low-frequency vibrations.

1. Introduction

After being proposed in 1968 [1], electromagnetic metamaterials with negative permittivity and permeability have been known for many years. In recent years some man-made materials with negative permeability were even experimentally verified [2]. Although metamaterials are made of conventional materials such as metal and plastic, they can exhibit unique properties which have not been found in nature. Famous properties of electromagnetic metamaterials include negative refractive indices [3], invisibility [4,5], and inverse Doppler effect [6]. These unique properties of electromagnetic metamaterials result from their designed periodic microstructures rather than chemical reactions during manufacturing. The shape, size, orientation and arrangement of the microstructures affect the transmission of light and create unnatural, unconventional material properties. Recently another type of metamaterials called acoustic metamaterials have been under widespread investigation [7–10]. An acoustic metamaterial structure can attenuate/stop or guide an elastic wave propagating in it along a desired path by employing the resonance between the integrated local microstructures and the propagating wave. For example, seismic waveguides are an important application of acoustic metamaterials. Earthquakes often cause dangerous elastic waves propagating in structural systems [11]. Based on characteristics of different seismic waves, Kim and Das proposed a novel seismic attenuator made of metamaterials [12].

Intensive studies on acoustic metamaterials began after the existence of acoustic metamaterials was analytically and experimentally verified [7]. Early studies on acoustic metamaterials focused on analysis of dispersion and stopband of simple mass-spring lattice structures because of easy modeling and manufacturing. In 2003 the phononic stopbands of 1-D and 2-D mass-spring lattice structures with two different types of working units were extensively investigated [13]. Influences of boundaries, viscous damping and imperfections were studied by analyzing a 1-D wave filter and a 2-D wave guide. Jensen concluded that the stopband of 1-D and 2-D structures based on type-1 working units was insensitive to damping and small imperfection, whereas the stopband of 2-D structures based on type-2

* Corresponding author.

http://dx.doi.org/10.1016/j.ijmecsci.2014.09.018
0020-7403/

working units was almost eliminated by strong damping. In 2003 different types of mechanical lattice structures with stopbands and the process of designing a lattice system with prescribed stopbands were proposed [14]. In 2007 the effect of attached mass-spring subsystems on a rigid body was investigated [15]. It was assumed that the attached masses were unknown to the observer and a dynamic effective mass of the rigid body was derived from a modified Newton's second law. They showed that the effective mass (called *p*-mass) was a function of vibration frequency and could be complex and huge near resonances. In 2008 the negative effective mass in a one-dimensional (1D) mass-spring system was experimentally confirmed [16]. A mass-spring unit was inserted into each subsystem and the subsystems were connected to each other by springs with different spring constants. The experiments were performed on an air track and CCD cameras were used to capture the motions of subsystems.

Although lattice structures with masses lumped at nodal points are easy to model, continuum structures like bars, beams and plates are more commonly used in real applications. In fact, the propagation of elastic waves in composite continuum structures is a traditional topic in material physics and acoustics. In 1994 the elastic wave propagation in infinite plates with periodic cylindrical inclusions was studied [17]. Unfortunately, the adopted plate theory based on continuum mechanics could not accurately model the local resonance of the attached microstructures. In 1998 a type of 2-D composite structures manufactured by inserting Duralumin cylindrical fibers into an epoxy matrix was proposed [18]. Experimental transmission spectra showed two stopbands within 55–85 kHz and 115–125 kHz for a finite-size sample with a square array of fibers. In 2008 a 1-D ultrasonic metamaterial beam showing simultaneously negative dynamic mass density and Young's modulus was reported [19]. The metamaterial beam was constructed by attaching Helmholtz resonators to an elastic beam. By treating the elastic beam and the Helmholtz resonators as a whole, finite element analysis using solid elements was conducted. The model was then improved by using parallel-coupled Helmholtz resonators [20]. However, the attached Helmholtz resonators need to be treated separately if accurate results are desired. In 2011 a plate model with mass-spring microstructures attached inside cavities was proposed [21]. Instead of using the traditional continuum mechanics theory to model the plate, they proposed a microstructure continuum theory that linearly extrapolated the spring–matrix interface points' displacements to represent displacements of the plate. This approach inappropriately assumed the displacements on the plate to be spatially linear and was not able to provide accurate solutions for the plate. In addition, the transverse motion of the plate was also unreasonably neglected. In 2010 a metamaterial bar composed by a hollow longitudinal bar with mass-spring subsystems attached inside was introduced [8]. Because the extended Hamilton principle [22] was used to model the whole integrated system, the so-obtained coupled system equations can provide accurate solutions of the metamaterial bar. Dispersion analysis and finite-element analysis showed that a stopband was created by the inertial forces of the attached subsystems and the stopband could be tuned by changing the resonant frequencies of the subsystems. A similar approach was taken to analyze a metamaterial beam manufactured by attaching translational and rotary inertias to an elastic beam [9]. Because shear deformation and rotary inertias can significantly affect propagation of high-frequency elastic waves within a beam, Timoshenko's beam theory and influences of rotary inertias were included in their modeling. Finite element analysis showed that a tunable stopband could be created by the attached inertias. However, translational inertias are far more efficient than rotary inertias for creating the stopband.

Possible applications of metamaterial plates are far more than those of metamaterial beams because structures are often majorly covered by plates with only few supporting beams inside. Potential applications of metamaterial plates include protection of important building structures (e.g., public administration offices, private office buildings, school buildings, and museums) during earthquakes, noise reduction for residential halls in busy cities and houses beside highways, etc. However, high-fidelity modeling and analysis of metamaterial plates is more challenging than that of metamaterial beams because of the increased order of dimension.

The objective of this work is to extend the concept of vibration absorbers to design acoustic metamaterial plates with wide stopbands to attenuate/stop high-frequency propagating waves and suppress low-frequency standing waves of plates. High-fidelity finite-element modeling is presented, and numerical analysis is performed to develop design guidelines. Moreover, the concepts of negative mass and stiffness are examined in detail, and influences of the absorbers' resonant frequencies and damping ratios and the plate's material damping and natural frequencies and mode shapes are investigated.

2. Concept of negative effective mass and stiffness

Electromagnetic metamaterials are based on negative permittivity and permeability to have unique unnatural material properties. Similarly, acoustic metamaterials are based on negative mass and stiffness to have unique unnatural material properties. To better understand the concept of negative mass and stiffness, we consider 2-DOF (degree of freedom) mass-on-mass and mass-on-spring vibration absorbers.

As shown in Fig. 1(a), the lumped mass m_2 is connected to the lumped mass $m_1 (> m_2)$ by a spring with a spring constant k. m_1 is subject to a force $f = f_0 e^{j\omega t}$, where $j \equiv \sqrt{-1}$ and ω is the excitation frequency. Equations of motion for this 2-DOF mass-on-mass vibration absorber are

$$\begin{bmatrix} m_1 & 0 \\ 0 & m_2 \end{bmatrix} \begin{Bmatrix} \ddot{u}_1 \\ \ddot{u}_2 \end{Bmatrix} + \begin{bmatrix} k & -k \\ -k & k \end{bmatrix} \begin{Bmatrix} u_1 \\ u_2 \end{Bmatrix} = \begin{Bmatrix} f \\ 0 \end{Bmatrix}, \quad f = f_0 e^{j\omega t} \tag{1}$$

where u_1 and u_2 are displacements of m_1 and m_2. If we define $\omega_1 \equiv \sqrt{k/m_1}$ and $\omega_2 \equiv \sqrt{k/m_2}$, the frequency response functions

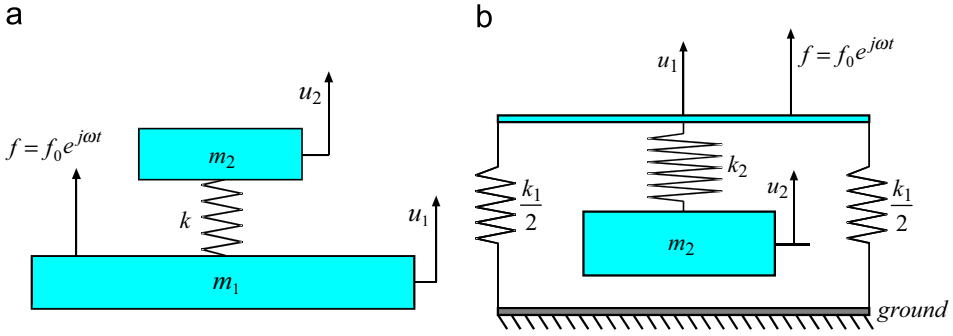

Fig. 1. Two-DOF vibration absorbers: (a) mass-on-mass absorber, and (b) mass-on-spring absorber.

(FRFs) $U_i(j\omega)$ of m_i can be obtained from Eq. (1) as

$$U_1(j\omega)=\frac{\omega_2^2-\omega^2}{\omega^2(\omega^2-\omega_1^2-\omega_2^2)}\frac{f_0}{m_1} \tag{2}$$

$$U_2(j\omega)=\frac{\omega_2^2}{\omega^2(\omega^2-\omega_1^2-\omega_2^2)}\frac{f_0}{m_1} \tag{3}$$

Eqs. (2) and (3) show that, if ω is within the open frequency range $(0,\omega_2)$, m_1 and m_2 move in phase and this is the so-called *acoustic mode*. On the hand, if ω is within $(\omega_2,\ +\infty)$, m_1 and m_2 are 180° out of phase and this is the so-called *optical mode*. If m_2 and the spring are hidden inside the mass m_1, the effective mass $\tilde{m}_1$ of the single-DOF system can defined and obtained to be

$$\tilde{m}_1\equiv\frac{f}{\ddot{u}_1}=\left(1+\frac{\omega_1^2}{\omega_2^2-\omega^2}\right)m_1 \tag{4}$$

Eq. (4) shows that $\tilde{m}_1$ is a function of ω. If $\omega\approx\omega_2$, $\tilde{m}_1\to\pm\infty$ and $u_1\approx 0$. This is because the force exerted on m_1 by m_2 balances with the excitation force and all the external energy is absorbed by m_2. If ω is within the frequency band $\left(\omega_2,\sqrt{\omega_1^2+\omega_2^2}\right)$, the effective mass is negative and m_1 and m_2 vibrate in an optical mode. Note that the negative effective mass occurs within a frequency band that is right at the higher side of the local resonant frequency ω_2 of the attached mass-spring subsystem.

Similar to the mass-on-mass system, Fig. 1(b) presents a mass-on-spring system. A massless rigid plate is connected to the ground by two springs having a spring constant $k_1/2$ and is excited by a force $f=f_0e^{j\omega t}$. The lumped mass m_2 is suspended below the rigid plate by a spring k_2. The displacements of the plate and m_2 are represented by u_1 and u_2. According to Newton's second law, equations of motion for this mass-on-spring vibration absorber are

$$\begin{bmatrix}0&0\\0&m_2\end{bmatrix}\begin{Bmatrix}\ddot{u}_1\\\ddot{u}_2\end{Bmatrix}+\begin{bmatrix}k_1+k_2&-k_2\\-k_2&k_2\end{bmatrix}\begin{Bmatrix}u_1\\u_2\end{Bmatrix}=\begin{Bmatrix}f\\0\end{Bmatrix},\ f=f_0e^{j\omega t} \tag{5}$$

From Eq. (5) we obtain the frequency response functions $U_i(j\omega)$ of m_i as

$$U_1(j\omega)=\frac{\omega_2^2-\omega^2}{k_1\omega_2^2-(k_1+k_2)\omega^2}f_0 \tag{6}$$

$$U_2(j\omega)=\frac{\omega_2^2}{k_1\omega_2^2-(k_1+k_2)\omega^2}f_0 \tag{7}$$

where $\omega_2\equiv\sqrt{k_2/m_2}$ is the local resonance frequency of the suspended mass-spring subsystem. If the suspended mass-spring subsystem is invisible to the observer, the 2-DOF system becomes a single-DOF system subject to a sinusoidal excitation force. Then, the effective spring constant $\tilde{k}_1$ of the new system can be defined and obtained as

$$\tilde{k}_1\equiv\frac{f}{u_1}=k_1+\frac{k_2}{1-(\omega_2/\omega)^2} \tag{8}$$

Eq. (8) indicates that $\tilde{k}_1$ is a function of ω. When $\omega\approx\omega_2$, $u_1\approx 0$ based on Eq. (6), i.e., the external excitation force is totally balanced out by the suspended mass-spring subsystem. Meanwhile, $\tilde{k}_1\to\pm\infty$ according to Eq. (8). If $\omega>\omega_2$, the plate and m_2 are 180° out of phase, i.e., an *optical mode*. Otherwise, when $\omega<\omega_2$, the plate and m_2 moves in phase, i.e., an *acoustic mode*. Moreover, when ω is within the frequency range $\left(\omega_2\sqrt{k_1/(k_1+k_2)},\omega_2\right)$, the effective stiffness is negative. Note that different from the mass-on-mass system, the negative effective stiffness of this mass-on-spring system happens in a frequency range right at the lower side of the local resonant frequency ω_2 of the attached mass-spring subsystem.

3. Dispersion analysis and elastic wave absorption

Based on the 2-DOF mass-on-mass vibration absorber, a metamaterial plate is proposed in Fig. 2. The metamaterial plate consists of two parallel isotropic plates and small mass-spring vibration absorbers integrated between the two plates. The vibration absorbers are mass-spring subsystems with mass and spring constants tuned to desired values. Except the clamped-free-free-free boundary conditions shown in Fig. 2, other types of boundary conditions can be assigned and studied. This kind of metamaterial plates is designed to guide elastic waves along a designated path within the plate. If damping is added to each vibration absorber, the guided waves can be attenuated/absorbed during their propagation.

A single-frequency elastic wave propagates with a specific phase velocity in a dispersive material. Dispersion analysis provides important information about how a single-frequency wave propagates along a certain direction in an infinite plate. If a plate is designed so that waves within a broad frequency band cannot propagate efficiently, then a wide-band wave absorber is designed. Because the mass-spring subsystems are periodically distributed over the plate, a unit cell (see Fig. 3) can be used to study by dispersion analysis how waves propagate in a plate without considering boundary conditions and size effects. A unit cell consists of two rectangular isotropic plates and a mass-spring subsystem inbetween. Its edge lengths along x and y directions are $2a$ and $2b$, respectively. Here we assume that the two springs have the same spring constant k, the absorber mass is $2m$, and the top and bottom plates move in phase and have the same magnitude of displacement. Considering this symmetric property, one can analyze only the upper half of the unit cell with an absorber mass of m and a spring constant k.

First we define moment resultants M_1, M_2 and M_6 as ([22])

$$M_1\equiv\int\sigma_{11}z\,dz=-D(w_{xx}+\nu w_{yy}),\quad M_2\equiv\int\sigma_{22}z\,dz=-D(\nu w_{xx}+w_{yy})$$
$$M_6\equiv\int\sigma_{12}z\,dz=-D(1-\nu)w_{xy},\quad D\equiv\frac{Eh^3}{12(1-\nu^2)} \tag{9}$$

where σ_{11} and σ_{22} are normal stresses along x and y directions, σ_{12} is the in-plate shear stress and w is the vertical displacement of the upper plate. The plate thickness, Poisson's ratio, Young's modulus and flexural rigidity are denoted by h, ν, E and D, respectively. Then the kinetic energy δT, elastic energy $\delta\Pi$ and non-conservative work δW_{nc} done by the external loads can be represented as

$$\delta T=\int_{-a}^{a}\int_{-b}^{b}(-\rho h\ddot{w}\delta w)\,dx\,dy \tag{10}$$

$$\delta\Pi=\int_{-a}^{a}\int_{-b}^{b}\int_{-h/2}^{h/2}(\sigma_{11}\delta\varepsilon_{11}+\sigma_{22}\delta\varepsilon_{22}+\sigma_{12}\delta\varepsilon_{12})\,dz\,dx\,dy$$
$$=\int_{-a}^{a}\int_{-b}^{b}(-M_{1xx}\delta w-M_{2yy}\delta w-2M_{6xy}\delta w)\,dx\,dy$$

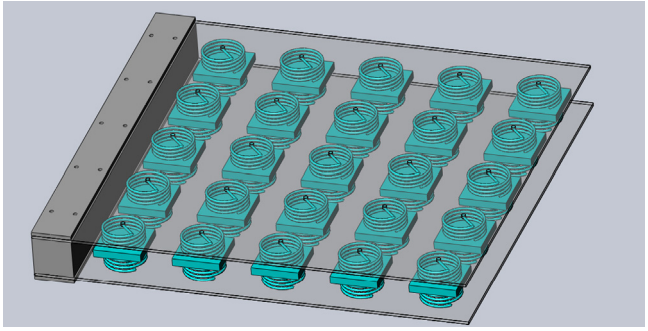

Fig. 2. A metamaterial plate with sping-mass subsystems.

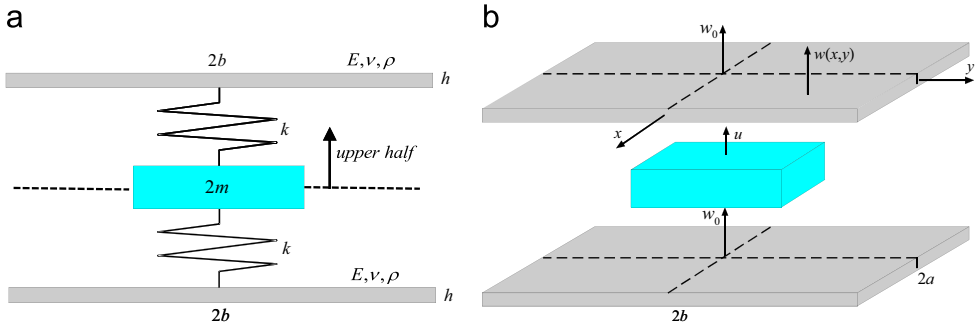

Fig. 3. A unit cell of the metamaterial plate: (a) front view, and (b) perspective view.

$$+\int_{-b}^{b}\Big\{\left[-M_1\delta w_x+(M_{1x}+M_{6y})\delta w-M_6\delta w_y\right]_{x=-a}^{x=0^-}+\left[-M_1\delta w_x+(M_{1x}+M_{6y})\delta w-M_6\delta w_y\right]_{x=0^+}^{x=a}\Big\}dy+\int_{-a}^{a}\Big\{\left[-M_2\delta w_y+(M_{2y}+M_{6x})\delta w-M_6\delta w_x\right]_{y=-b}^{y=0^-}+\left[-M_2\delta w_y+(M_{2y}+M_{6x})\delta w-M_6\delta w_x\right]_{y=0^+}^{y=b}\Big\}dx \tag{11}$$

$$\delta W_{nc}=\int_{-b}^{b}\left[-M_1\delta w_x+Q_1\delta w-M_6\delta w_y\right]_{x=-a}^{x=a}dy+\int_{-a}^{a}\left[-M_2\delta w_y+Q_2\delta w-M_6\delta w_x\right]_{y=-b}^{y=b}dx+k(u-w_0)\delta w_0$$
$$(Q_1=M_{1x}+M_{6y},\,Q_2=M_{2y}+M_{6x}) \tag{12}$$

The vertical force resultants are represented by Q_1 and Q_2. Substituting Eqs. (10)–(12) into the extended Hamilton principle yields

$$0=\int_0^t(\delta T-\delta\Pi+\delta W_{nc})dt=\int_0^t\left\{\int_{-a}^{a}\int_{-b}^{b}\left(-\rho h\ddot{w}+M_{1xx}+M_{2yy}+2M_{6xy}+\left[\tilde{Q}+k(u-w_0)\right]\delta(x,y)\right)\delta w\,dx\,dy\right\}dt$$
$$\tilde{Q}\equiv\left(Q_1^{x=\varepsilon_1/2}-Q_1^{x=-\varepsilon_1/2}\right)\varepsilon_2+\left(Q_2^{y=\varepsilon_2/2}-Q_2^{y=-\varepsilon_2/2}\right)\varepsilon_1,\quad \varepsilon_1,\varepsilon_2\approx 0 \tag{13}$$

where $\delta(x,y)$ is a 2D Dirac delta function, and $\tilde{Q}$ represents the discontinuity of the internal transverse shear force at the absorber location. Setting the coefficient of δw to zero yields the plate's governing equation as

$$-\rho h\ddot{w}+M_{1xx}+M_{2yy}+2M_{6xy}+\left[\tilde{Q}+k(u-w_0)\right]\delta(x,y)=0 \tag{14}$$

The governing equation of the vibration absorber can be readily obtained from Newton's second law as

$$m\ddot{u}=k(w_0-u) \tag{15}$$

Integration of Eq. (14) across the upper plate gives

$$0=\int_{-a}^{a}\int_{-b}^{b}\left\{-\rho h\ddot{w}+M_{1xx}+M_{2yy}+2M_{6xy}+\left[\tilde{Q}+k(u-w_0)\right]\delta(x,y)\right\}dx\,dy=\int_{-a}^{a}\int_{-b}^{b}(-\rho h\ddot{w})\,dy\,dx+\int_{-a}^{a}(M_{2y}+M_{6x})_{y=-b}^{y=b}dx+\int_{-b}^{b}(M_{1x}+M_{6y})_{x=-a}^{x=a}dy+k(u-w_0) \tag{16}$$

Note that $\tilde{Q}$ is canceled out. Eq. (16) is equivalent to treating the upper plate as a rigid body moving at an acceleration averaged over the $2a\times 2b$ area and subject to transverse shear forces on the four edges and a concentrated center force from the absorber. In other words, it is treated as a dynamically equivalent 2-DOF system (i.e., the plate and the absorber), but the plate's equivalent dynamic mass is deformation-dependent. If the bottom plate's displacement in Fig. 3b is allowed to be different from that of the top plate, the problem can be similarly analyzed but the number of DOFs increases from two to three.

If a single-frequency 2D elastic wave propagates within an infinite metamaterial plate made of many of the above analyzed unit cell (see Fig. 3b), the plate's displacement w and the absorber's displacement u can be assumed to have the following forms:

$$w=pe^{j(\alpha x+\beta y-\omega t)},\quad u=qe^{-j\omega t} \tag{17}$$

where $\alpha(\equiv 2\pi/\lambda_1)$ and $\beta(\equiv 2\pi/\lambda_2)$ are wavenumbers along the x and y directions with λ_1 and λ_2 being the corresponding wave lengths, ω is the wave frequency, and p and q are displacement amplitudes. Substituting Eq. (17) into Eqs. (15) and (16) and rewriting the results in a matrix form gives

$$\begin{bmatrix}\frac{\sin(a\alpha)\sin(b\beta)}{\alpha\beta}\left[4\rho h\omega^2-4D\left(\alpha^2+\beta^2\right)^2\right]-k & k\\ k & m\omega^2-k\end{bmatrix}\begin{Bmatrix}p\\ q\end{Bmatrix}=0 \tag{18}$$

To have non-zero solutions to the eigenvalue problem shown in Eq. (18), the determinant of the matrix needs to be zero and hence the dispersion equation that relates ω to α and β (i.e., the 2D wave vector) is obtained as

$$(m\omega^2-k)\left\{\frac{4\sin(a\alpha)\sin(b\beta)}{\alpha\beta}\left[\rho h\omega^2-D\left(\alpha^2+\beta^2\right)^2\right]-k\right\}-k^2=0 \tag{19}$$

if ω is assumed to be real and positive, solving Eq. (19) yields the two solutions of ω in terms of α and β (i.e., dispersion surfaces) as shown in Fig. 4, where we choose

$2a=0.25\ m,\ 2b=0.05\ m,\ h=0.015\ \text{m},\ m=75\ \text{g},\ \sqrt{k/m}=500\ \text{Hz}$

Young's modulus : $E=72.4$ GPa,

Poisson ratio : $\nu=0.33$, mass density : $\rho=2800\ \text{kg/m}^3$

Fig. 4(b) shows the front view of Fig. 4(a). There is a stopband between 500 Hz and 534.5 Hz (the gray band in Fig. 4(b)) where no wave can propagate forward. The upper bound of the stopband is obtained from the upper dispersion surface with α and $\beta\to 0$ and the lower bound from the lower dispersion surface with α and $\beta\to\infty$ as.

$$\text{Stopband}=\left(\sqrt{k/m},\sqrt{k/m+k/(4abh\rho)}\right) \tag{20}$$

where $4abh\rho$ is the mass of the plate's unit cell. Eq. (20) shows that the stopband's width can be increased by reducing the ratio $4abh\rho/m$. However, a small $4abh\rho/m$ value means a big absorber

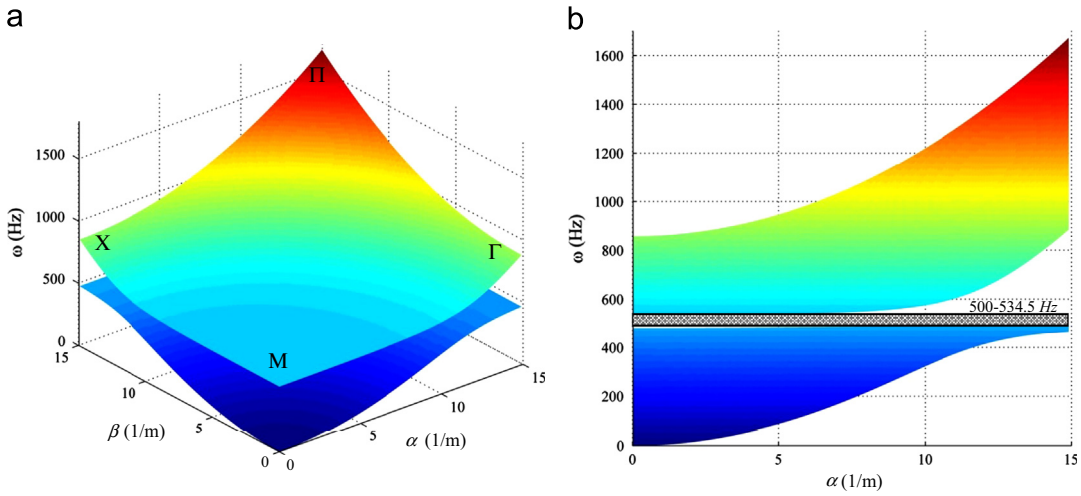

Fig. 4. Dispersion surfaces and stopband: (a) dispersion surfaces, and (b) stopband (gray rectangle).

mass, which is bad for design because the absorbers are too heavy. The stopband is just right above the absorber's local resonance frequency (i.e., $\sqrt{k/m}$) because the absorber's resonant vibration generates a significant out-of-phase inertial force to counteract the plate's internal shear force, straighten the plate, and stop wave propagation. This is analogous to the working mechanism of the 2-DOF mass-on-mass system shown in Fig. 1(a). If proper damping is added to the vibration absorbers, energy of elastic waves with frequencies within the stopband can be efficiently absorbed into the absorbers and damped out. Proper selection and distribution of vibration absorbers with different local resonant frequencies will enable design of broad-band waveguides. However, this dispersion analysis is only valid for infinite plates. For finite plates, finite-element modeling of the whole metamaterial plate is needed, as shown next.

4. Finite-element modeling and frequency response analysis of metamaterial plates

One important application of metamaterials is for absorption/attenuation of destructive propagating waves in a plate caused by earthquake or explosion. For elastic waves, an appropriately designed metamaterial-based plate in a structural system (e.g., a building with several walls) can attenuate them, guide them away from main structural components (e.g., pillars in a wall), and/or delay them from reaching main components before being significantly attenuated by vibration absorbers. Then, the structural system's main components can survive although some secondary components may be damaged. To demonstrate the concept we consider the metamaterial plate shown in Fig. 5, which has the following dimensions and material properties:

Each plate : $L_a = 5$ m along x, $L_b = 3$ m along y, $h = 1.5$ cm

$E = 72.4$ GPa, $\nu = 0.33$, $\rho = 2800$ kg/m^3

Distance between top and bottom plates : $H = 20$ cm

Absorbers : $2m = 0.15$ kg, $\sqrt{2k/2m} = 500$ Hz

The metamaterial plate consists of two isotropic plates and mass-spring subsystems and is located between two hinged vertical pillars at $x=0$ and 5 m. The total mass of the subsystems is 11.5% of the total mass of the metamaterial plate. The same harmonic excitation force with an amplitude of 100 kN is applied at $x=5$ cm and $y=1.5$ m (i.e., the green dot in Fig. 5(b)) on both plates. Each plate is modeled by 100×12 four-node rectangular conforming

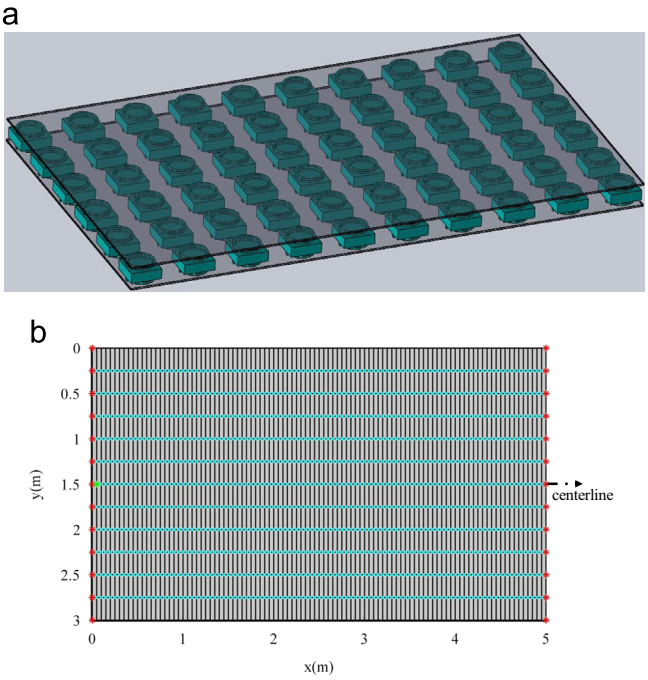

Fig. 5. A metamaterial plate with two edge hinged: (a) a 3D model, and (b) a finite-element model.(For interpretation of the references to color in this figure legend, the reader is referred to the web version of this article.)

plate elements with four DOFs (w, $w_x(\equiv \partial w/\partial x)$, w_y and w_{xy}) at each node. Because the wave propagation along x is of great interest here, fine meshes are used along x. The vibration absorbers are between the two plates and are attached to the plate elements' nodes. However, there are no absorbers on the two free edges at $y=0$ and 3 m. The unit cell here has the same size and parameters as those used in the dispersion analysis presented in Fig. 4. Based on the dispersion analysis presented in the previous section for an infinite plate, a stopband between 500 Hz and 534.5 Hz exists if the vibration absorbers are tuned to have $\sqrt{k/m} = 500$ Hz and the boundary effect is neglected.

The steady-state response of a metamaterial plate under a harmonic excitation can be predicted by frequency response analysis (FRA). Although the displacements of the top and bottom plates can be different under a general excitation, we consider here that the same harmonic excitation is applied on the two plates at the same location. Hence, the two plates have the same

motion for this case here. Two representative frequency response functions (FRFs) of the metamaterial plate are shown in Fig. 6. The black dotted lines are for the metamaterial plate without vibration absorbers (setting $m=0$) and are plotted for reference. The red lines show FRFs of the plate with a low damping ratio $\varsigma=0.0001$ for each vibration absorber. After increasing the damping ratio to 0.01, FRFs are shown by the blue lines. The red lines show a stopband to the right side of 500 Hz, as predicted by dispersion analysis. When the excitation frequency approaches the stopband, the vibration absorbers are close to resonant vibration and many response peaks appear around the stopband. Fortunately, these response peaks can be lowered and smoothed by increasing the damping of the vibration absorbers. Damping in vibration absorbers can efficiently lower the response in low-frequency areas and broaden the stopband at the same time, as shown by the blue lines in Fig. 6. In other words, a metamaterial plate with high damping absorbers can stop propagating high-frequency elastic waves within the stopband, and it can also suppress standing low-frequency vibrations below the stopband, which is different from a metamaterial beam ([9]). These characteristics are very favorable for designing metamaterial plates for both elastic wave absorption and structural vibration suppression. Unfortunately, high damping does not significantly reduce the response in areas of frequencies higher than the stopband, and it often increases the transient time during startup and shutdown of the excitation. This characteristic may decrease the efficiency of or even disable the absorbers. To examine this phenomenon and to determine an appropriate damping value for vibration absorbers, transient analysis by direct numerical integration of the finite-element equations is needed, as shown next.

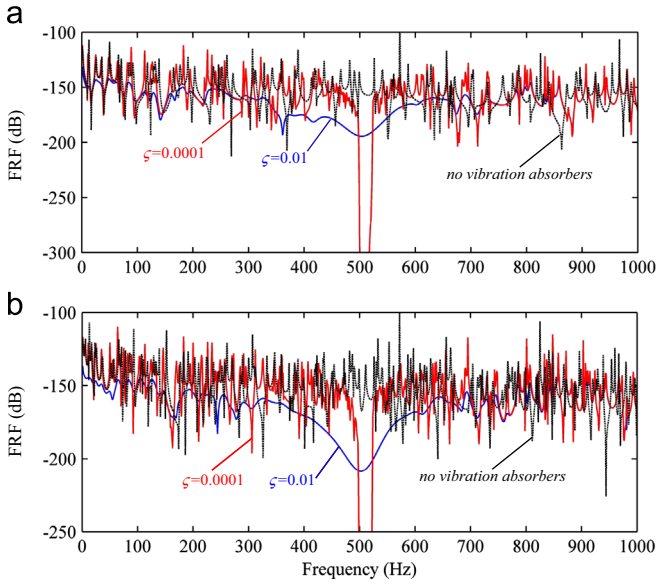

Fig. 6. Frequency response functions of the metamaterial plate: (a) response at $x=0.5L_a$ and $y=0.5L_b$, and (b) response at $x=0.8L_a$ and $y=0.5L_b$.(For interpretation of the references to color in this figure legend, the reader is referred to the web version of this article.)

The above results from FRA give information about the steady-state performance of the metamaterial plate. But how an elastic wave propagates during the transient period and how the transient parts are damped out need to be examined through transient analysis. If the natural frequency of vibration absorbers is tuned to be 500 Hz, a constant damping ratio of 0.01 is used for each

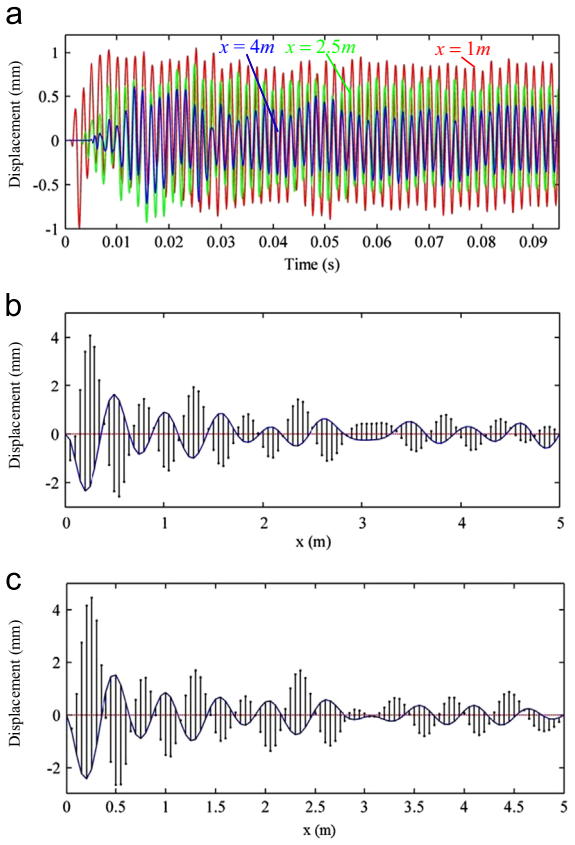

Fig. 7. Transient analysis under $\omega=600$ Hz: (a) vibrations of nodes at $x=1$ m, 2.5 m, 4 m on the centerline, (b) ODSs from direct numerical integration, and (c) ODSs from FRA.

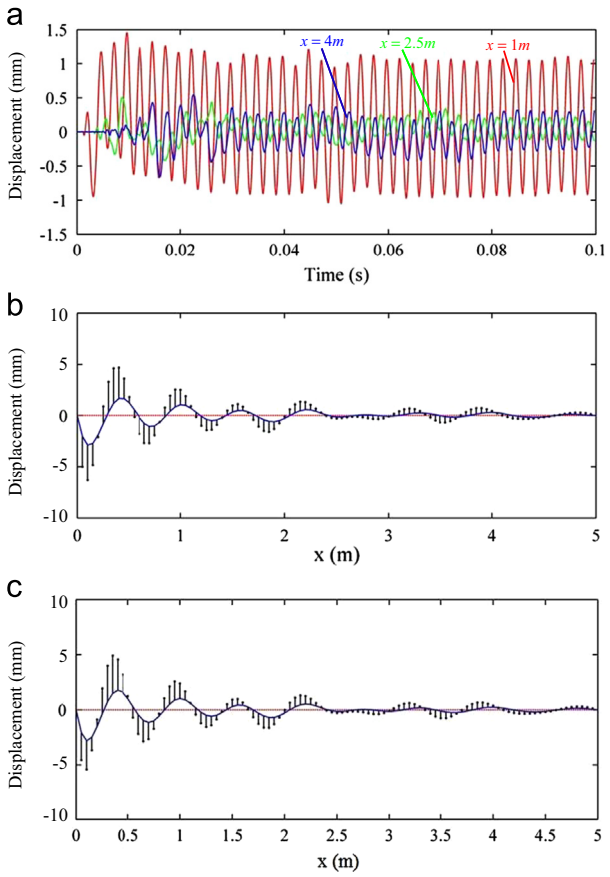

Fig. 8. Transient analysis under $\omega=400$ Hz: (a) vibrations of nodes at $x=1$ m, 2.5 m, 4 m on the centerline, (b) ODSs from direct numerical integration, and (c) ODSs from FRA.

vibration absorber, the external excitation frequency ω is set at 600 Hz, and a time step $\Delta t = 0.0001$ s is used for numerical integration, Fig. 7(a) shows the transient vibrations of nodes at $x=1$ m, 2.5 m and 4 m on the centerline ($y=1.5$ m, see Fig. 5(b)). Note that, when the excitation starts, the wave propagates through the surrounding media and passes the nodes at $x=1$ m, 2.5 m, 4 m on the centerline. It takes about 0.005 s for the wave to reach the node at $x=4$ m and hence the wave speed is about 800 m/s. A steady state is reached around 0.1 s. Fig. 7(b) shows the operational deflection shapes (ODSs) of the plate and vibration absorbers on the centerline ($y=1.5$ m) when the node at $x=1.5$ m reaches its maximum displacement around $t=0.095$ s (i.e., the end of numerical integration). Because the excitation frequency is far away from the stopband (500 Hz–534.5 Hz), the wave can propagate forward as shown in Fig. 7(b). However, Fig. 7(a) and (b) shows that the influences of damping and boundary conditions are significant because the plate's vibration amplitude decreases as the wave propagates forward and the wave is reflected back after reaching the right-side boundary. More simulations reveal that influences of damping and boundary conditions are strong when the excitation frequency is around the first few natural frequencies of the structure, which agrees with the results shown in Fig. 6. Because the excitation frequency (600 Hz) is higher than the local resonant frequency of vibration absorbers, the system vibrates in an optical mode, i.e., motions of the plate and vibration absorbers are 180° out of phase. Fig. 7(c) shows the ODS from FRA for comparison. Note that Fig. 7(b) agrees fairly well with Fig. 7(c), except some subtle differences near the right boundary. In other words, it confirms that the metamaterial plate can reach a steady state within 0.1 s (about 60 excitation periods).

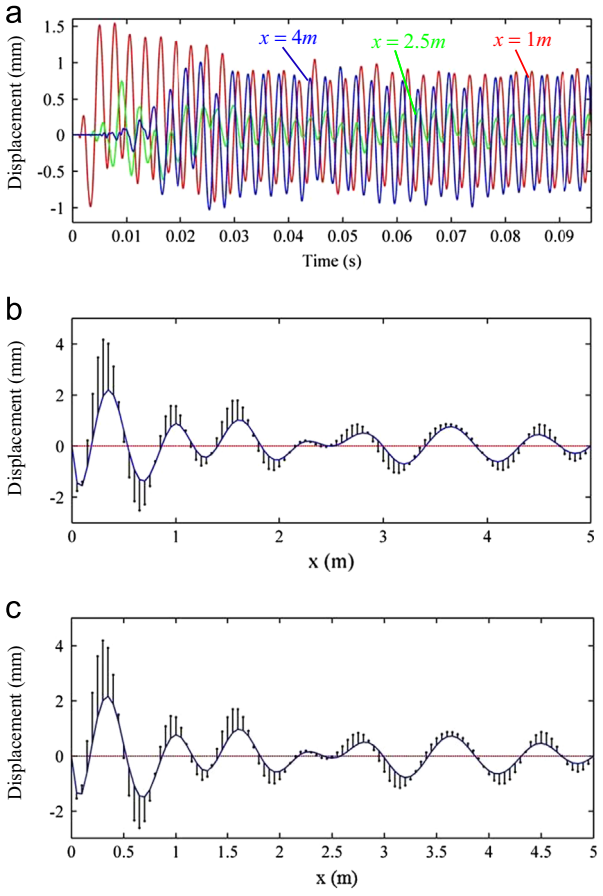

Fig. 9. Transient analysis under $\omega=350$ Hz: (a) vibrations of nodes at $x=1$ m, 2.5 m, 4 m on the centerline, (b) ODSs from direct numerical integration, and (c) ODSs from FRA.

Similar to Fig. 7, Fig. 8 shows the results under a harmonic excitation at $\omega=400$ Hz. Because the excitation frequency is lower than the local resonant frequency of vibration absorbers, the structure vibrates in an acoustic mode, i.e., the wall and the vibration absorbers move in phase. It takes about 0.1 s (40 excitation periods) for the structure to reach a steady state. One should note that, although the excitation frequency is much lower than the stopband, Fig. 8(b) shows that the vibration absorbers still can attenuate the wave. This is because the stopband obtained from dispersion analysis is based the assumptions of no damping and no boundary (i.e., an infinite plate). The FRFs shown in Fig. 6 include the influences of boundaries and damping, and they show that the structure should have a small vibration amplitude at $\omega=400$ Hz. Fig. 9 shows the results under a harmonic excitation at $\omega=350$ Hz. The vibration absorbers move in phase with the wall (i.e., acoustic mode) and cannot stop the wave propagation, which agrees with the dispersion analysis.

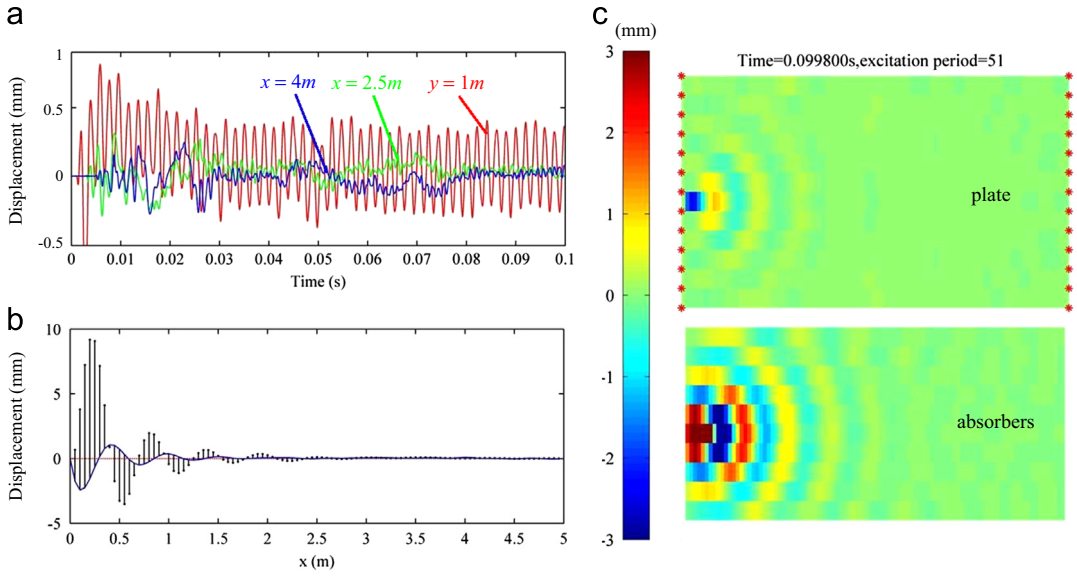

Fig. 10. Transient analysis under $\omega=510$ Hz: (a) vibrations of nodes at $x=1$ m, 2.5 m, 4 m on the centerline, (b) ODSs of the plate's centerline from direct numerical integration, and (c) ODSs of the whole plate (top) and absorbers (bottom).

The case with $\omega=510$ Hz (within the stopband) is shown in Fig. 10. It takes about 0.1 s (51 excitation periods) to reach the steady state. Because the excitation frequency falls within the stopband, both the wall and vibration absorbers at $x>2$ m have almost no vibration. The plate and vibration absorbers work in a mixed mode (containing both optical and acoustic modes). Fig. 10(c) depicts the ODSs of the plate (top plot) and absorbers (bottom plot). Displacements of absorbers are measured relative to the average displacement of the top and bottom plates. Fig. 11 shows the distributions of shear force intensities along the centerline of the structure when the structure reaches the steady state. The shear force intensities on the yz and xz cross-sections are denoted by Q_1 and Q_2, respectively. Because waves on the plate's centerline at $y=1.5$ m primarily propagate along the x axis, Q_1 is much larger than Q_2, as shown in Fig. 11(b) and (c). Due to the concentrated excitation force, Q_1 and Q_2 at $x=0.05$ m have large magnitudes and significant discontinuity. The vertical broken red lines in Fig. 11(a) and (b) indicate that peak internal shear forces always occur around where vibration absorbers move opposite to the plate with peak amplitudes. In other words, the inertial forces from the vibration absorbers in resonant vibration

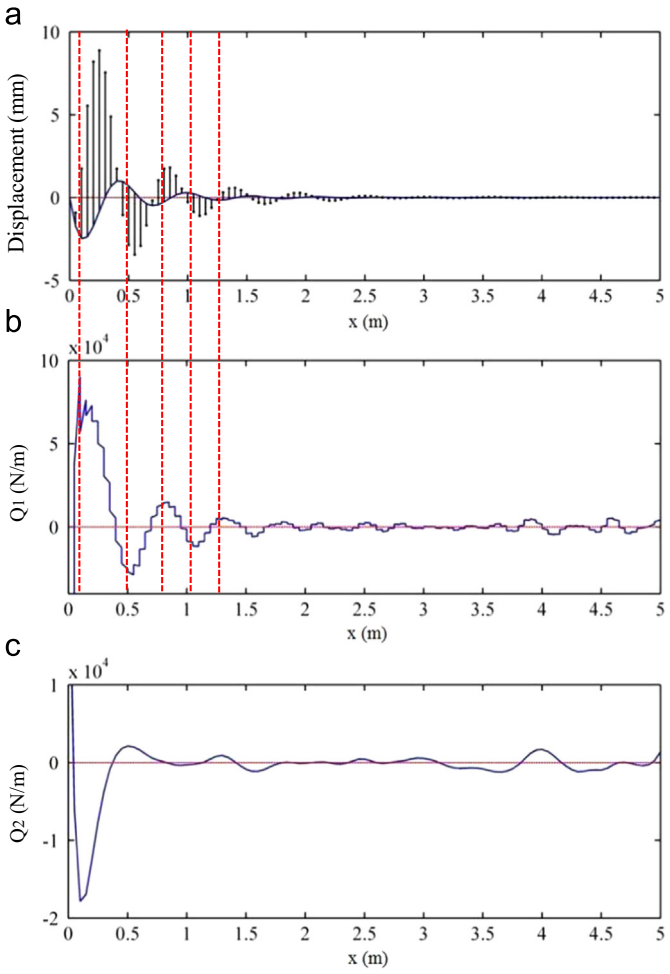

Fig. 11. ODSs and internal shear forces along the centerline: (a) ODSs, (b) shear force intensity Q_1, and (c) shear force intensity Q_2.(For interpretation of the references to color in this figure legend, the reader is referred to the web version of this article.)

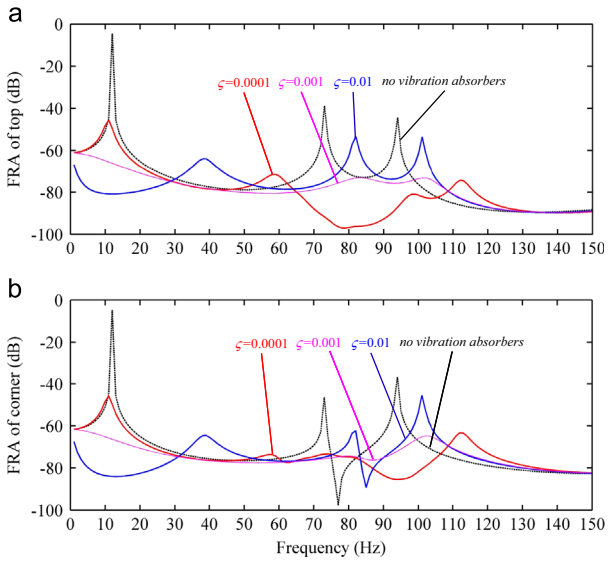

Fig. 13. FRFs of the low-frequency metamaterial plate with different damping ratios for vibration absorbers: (a) the top node at $x=0.25$ m and $y=0.5$ m , and (b) the corner node at $x=0$,0.5 m and $y=0.5$ m.(For interpretation of the references to color in this figure legend, the reader is referred to the web version of this article.)

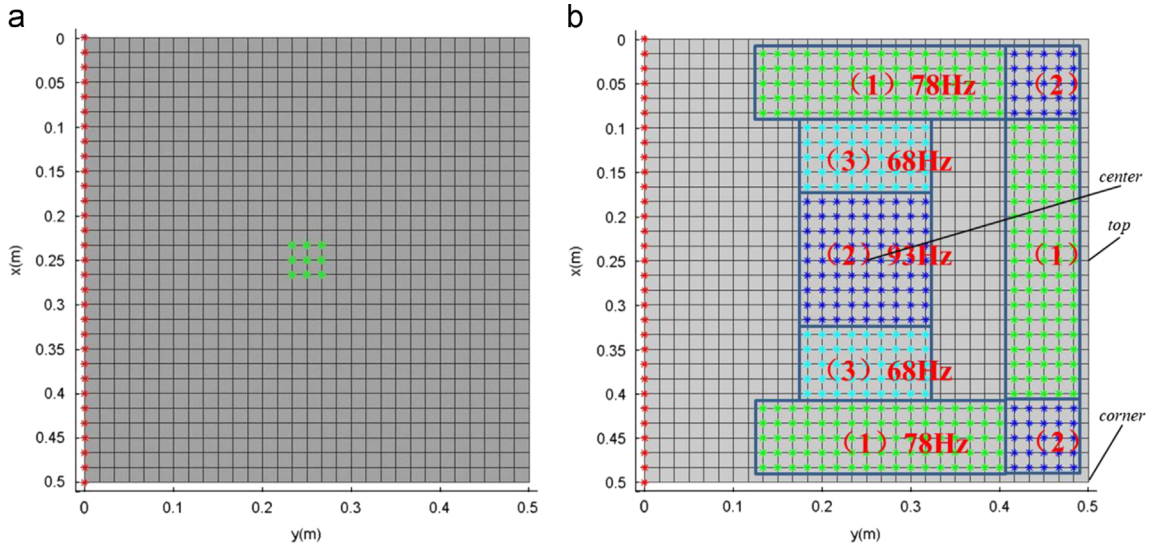

Fig. 12. A low-frequency metamaterial plate: (a) finite-element mesh, and (b) distribution of vibration absorbers of different resonant frequencies.(For interpretation of the references to color in this figure legend, the reader is referred to the web version of this article.)

balance out the plate's internal shear forces and straighten the plate to stop the wave propagation. This is the main working mechanism of metamaterial plates, rather than the concept of negative mass and/or stiffness as for metamaterials bars [8].

5. Design for low-frequency vibration suppression

Waves in metamaterial plates generated by low-frequency excitation are strongly affected by absorbers' resonant frequencies, damping ratios and locations as well as the plate's boundary conditions and low-order natural frequencies and mode shapes., damping ratios, location and distance between the vibration absorbers, vibration modes of the structures etc. Therefore different structures under different working conditions should be taken care of differently. By selecting appropriate masses and springs for vibration absorbers and properly locating them on the metamaterial plate, one can design a low-frequency metamaterial plate with a wide stopband and the vibration of the structure can be suppressed. In order to avoid adding too much mass to the original structure, the masses are designed to be 1.5 g for each vibration absorbers. Because the total mass of absorbers is required to be around 10% of the metamaterial plate mass, the mass of the vibration absorbers is maintained constant and the spring constants are adjusted to change the natural frequency of the vibration absorbers. In most cases, it is not necessary to put the

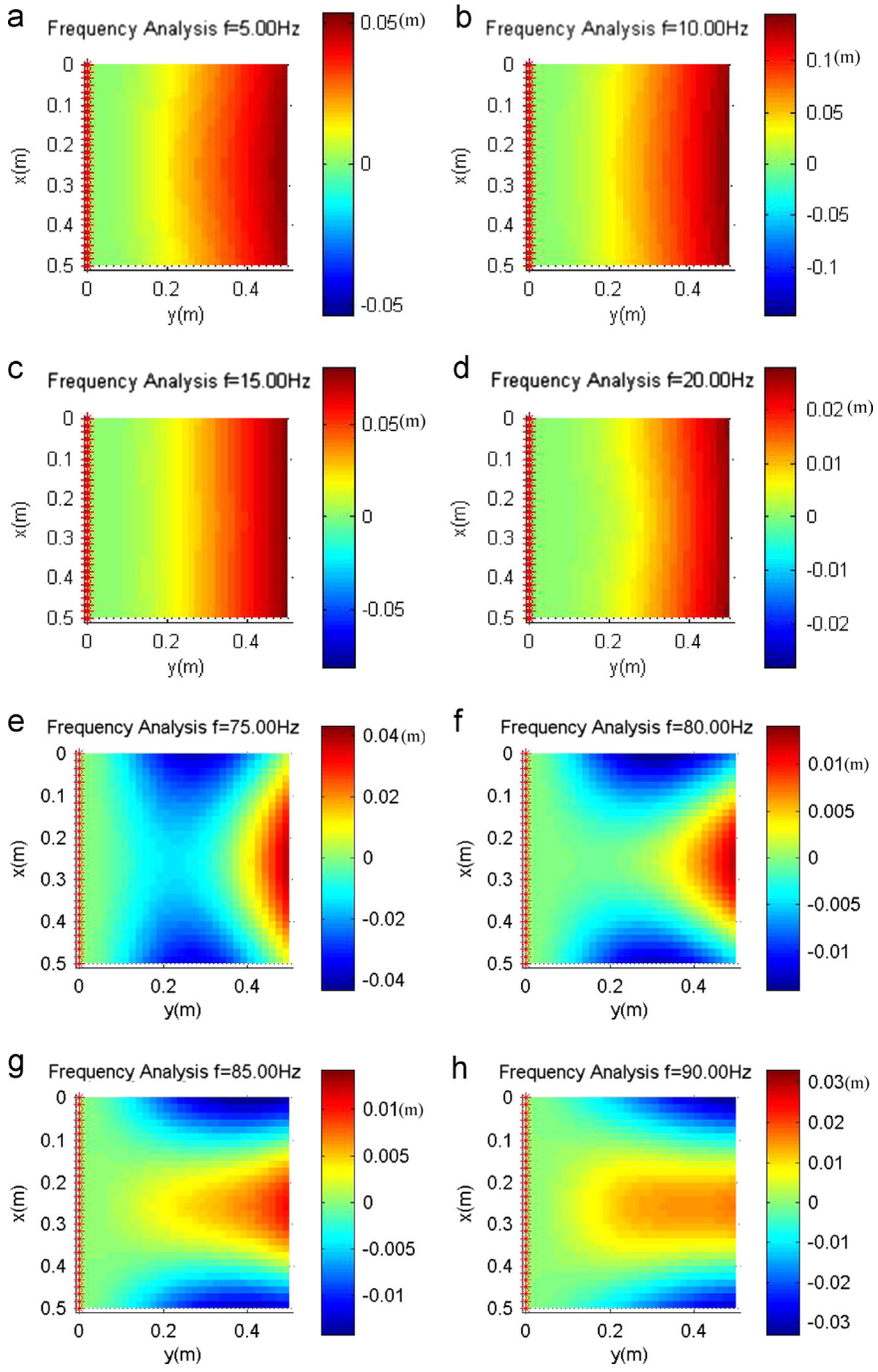

Fig. 14. FRFs of the low-frequency metamaterial plate without vibration absorbers: (a)–(d) single-frequency excitations around 10 Hz, and (e)–(h) single-frequency excitations around 80 Hz.

vibration absorbers uniformly across the plates. A metamaterial plate for low-frequency vibration suppression is shown in Fig. 12. The metamaterial plate consists of two isotropic plates and mass-spring subsystems are located between the two plates (see Fig. 2). Clamped-free-free-free boundary conditions are considered here. If not otherwise stated, the material properties and dimensions of the metamaterial plate are

Each plate : 0.5 m along x, 0.5 m along y, $h=3.5$ mm

$E=72.4$ GPa, $\nu=0.33$, $\rho=2800$ kg/m^3

Distance between top and bottom plates : $H=5$ cm

Absorbers mass : $2m=1.5$ g

Because the excitation location only slightly affects a vibration mode shape around a plate's resonant frequency, a harmonic force with amplitude of 50 N is applied at the plate's center area (i.e., green dots in Fig. 12(a)) on both isotropic plates. In order to find the peak response of the metamaterial plate and appropriately arrange/design the locations and resonant frequencies of vibration absorbers, frequency response analysis (FRA) on the metamaterial plate without vibration absorbers should be conducted first. As shown in Fig. 12(a), 30×30 rectangular conforming plate elements with four DOFs (w, w_x, w_y and w_{xy}) at each node are used. The dotted black lines in Fig. 13 represent the FRFs of the top and corner nodes (see Fig. 12(b)) of the metamaterial plate without vibration absorbers (setting $m=0$). The first natural frequency is around 10 Hz (called the low band hereafter) and the second and third natural frequencies are around 75–95 Hz (called the high band hereafter). Fig. 14(a)–(d) and (e)–(h) shows the ODSs under an excitation frequency around the low and high bands, respectively. They all show large vibration amplitudes, but later simulations will show that vibrations around the low band can be effectively suppressed by adding damping to absorbers.

The ODS at 75 Hz in Fig. 14(e) shows that large vibration amplitudes appear around the three free edges, and the ODS at 90 Hz in Fig. 14(h) shows that large amplitudes appear around the two free corners and the central part of the metamaterial plate. Therefore, the first group of vibration absorbers with a resonant frequency of 78 Hz (i.e., green dots in Fig. 12(b)) is placed around the three free edges, and the second group of absorbers with a resonant frequency of 93 Hz (i.e., blue dots in Fig. 12(b)) is placed around the center and the two free corners. After adding these two groups of absorbers, FRA is conducted again and results show that the central part under an excitation frequency of 70 Hz has a large vibration amplitude. Therefore, a third group of absorbers with a resonant frequency of 68 Hz (i.e., cyan dots in Fig. 12(b)) is placed around the center. After adding the three groups of absorbers, the total mass of the vibration absorbers is 13% of the plate's mass. The red lines in Fig. 13 show that, using $\varsigma=0.0001$ for vibration absorbers, the plate's vibration amplitude around 80 Hz is significantly reduced. Fig. 15(a) compares the ODSs of the plate under a 90 Hz excitation without and with vibration absorbers, and Fig. 15(b) shows the results under a 95 Hz excitation. Apparently, the significant vibration suppression is due to the vibration absorbers having appropriately tuned local resonant frequencies and locations. In other words, it is caused by the existence of a stopband around 75–95 Hz, as shown in Fig. 13.

When $\varsigma=0.01$ is used for vibration absorbers, the blue lines in Fig. 13 show that, although the response amplitude around 10 Hz is well reduced but the response amplitude around 80 Hz dramatically increases from that with $\varsigma=0.0001$. In other words, the stopband effect is destroyed by the high damping of vibration

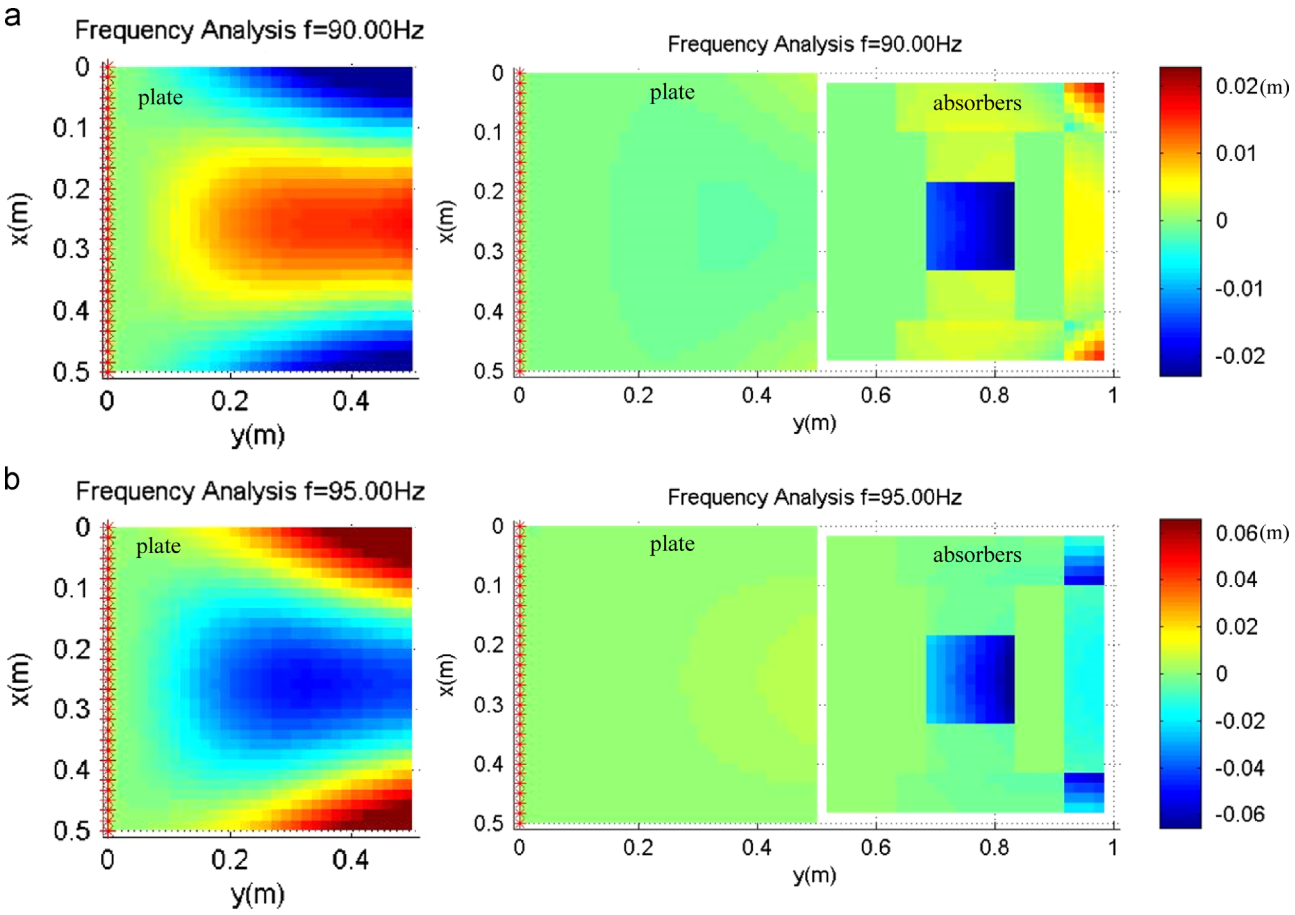

Fig. 15. ODSs of the metamaterial plate without (left) and with (right) vibration absorbers with $\varsigma=0.0001$: (a) 90 Hz excitation, and (b) 95 Hz excitation.

absorbers. This is because the high damping prevents the vibration energy from transferring into the vibration absorbers. Hence, a proper damping value must be determined in order to keep the stopband effect and remain the capability of suppressing low-band vibrations. With the use of $\varsigma = 0.001$, the magenta lines in Fig. 13 show that both response amplitudes around low and high bands are significantly reduced. Hence the following guidelines for designing a low-frequency metamaterial plate are proposed: (1) conducting FRA on a proposed metamaterial plate without vibration absorbers, (2) determining the resonant frequencies and locations of vibration absorbers based on the first few natural frequencies and mode shapes of the plate, (3) conducting FRA on the metamaterial plate with added vibration absorbers and making improvement if necessary, and (4) adding appropriate damping to the vibration absorbers.

In order to better understand how different dampings affect performance of the low-frequency metamaterial plate shown in Fig. 12(b), transient analysis by direct numerical integration is conducted. Fig. 16(a) shows the transient vibrations of the corner, top and center nodes under a 90 Hz excitation and modal damping ratios [23] $\varsigma_1, \ldots, \varsigma_n = 0.05 : (0.005 - 0.05)/(n-1) : 0.005$ being used for the top and bottom plates, where n is the total number of DOFs of the finite-element model. Note that the first modal vibration around 10 Hz persists for a long while before being damped out although a large modal damping ratio of 0.05 is used for the first mode. In other words, the material damping of the structure itself is not efficient for vibration suppression. Moreover, natural structural materials with high material damping are not commonly available. On the other hand, because vibration absorbers are discrete man-made mass-spring subsystems, damping can be easily added and adjusted according to practical needs. Fig. 16(b) shows the transient vibrations when $\varsigma = 0.02$ is used for each vibration absorber and no damping for plates. It is obvious that the first modal vibration is quickly damped out and a steady-state harmonic vibration at the excitation frequency with an amplitude much less than that in Fig. 16(a) is achieved within less than 0.6 s. Fig. 16(c) shows the transient vibrations when $\varsigma = 0.02$ is used for each vibration absorber and the above modal damping ratios are used for the two plates. The differences between Fig. 16(b) and (c) are small. This indicates that the damping of the structure itself is not as efficient as the damping of vibration absorbers.

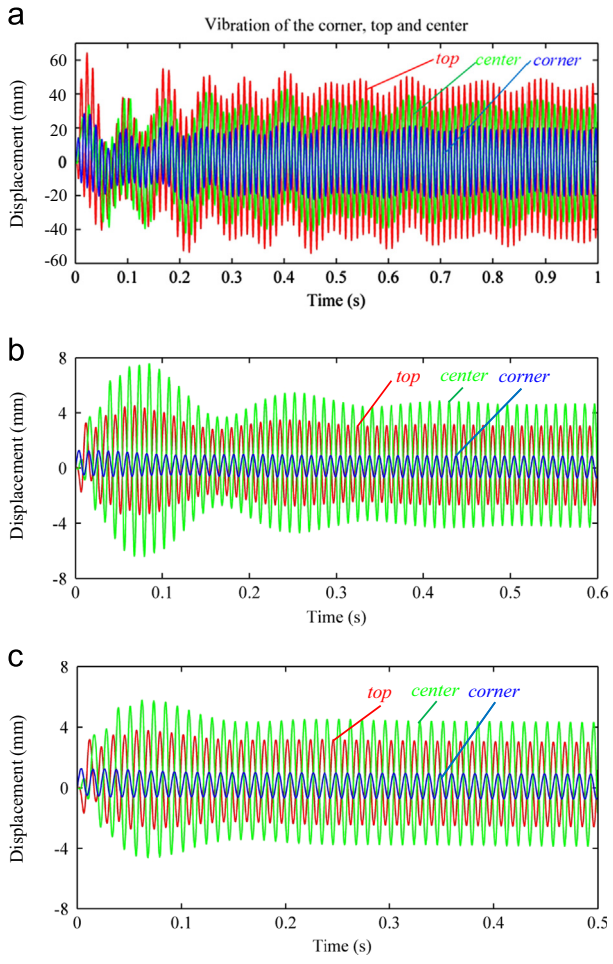

Fig. 16. Transient responses of the metamaterial plate with: (a) plate's modal damping ratios, (b) vibration absorbers' damping ratio $\varsigma = 0.02$, and (c) both plate's modal damping ratios and vibration absorbers' damping ratio $\varsigma = 0.02$.

6. Conclusions

This paper presents detailed modeling approach, analysis methods, and guidelines for designing acoustic metamaterial plates for both high-frequency elastic wave absorption and low-frequency structural vibration suppression. The design analysis includes analytical dispersion analysis, finite-element modeling, frequency response analysis, and direct numerical integration of finite-element equations. Acoustic metamaterial plates with integrated mass-spring subsystems are shown to be based on the concept of conventional vibration absorbers. The key working mechanism is that the local resonant vibration excited by the incoming elastic wave absorbs the vibration energy and creates a concentrated force to straighten the plate and attenuate/stop the propagating wave. Numerical results reveal that the stopband's location on the frequency axis is determined by the local resonant frequency of absorbers, and the stopband's width is determined by the absorber-mass/unit-plate-cell-mass ratio. Increase of absorbers' damping can increase the stopband's width and reduce low-frequency vibration amplitudes, but too much damping may deactivate the stopband effect. Increase of the plate's material damping through the use of modal damping ratios can also achieve the same effect, but it is far less efficient than absorbers' damping. The resonant frequencies, locations and distributions of absorbers need to be determined by considering the whole metamaterial plate's low-order natural frequencies and mode shapes under specific boundary conditions in order to have efficient low-frequency vibration suppression for each specific structural system.

References

[1] Veselago VG. The electrodynamics of substances with simultaneously negative values of permittivity and permeability. Soviet Physics Uspekhi 1968;10:509–14.
[2] Smith DR, Padilla WJ, Vier DC, Nemat-Nasser SC, Schultz S. Composite medium with simultaneously negative permeability and permittivity. Phys Rev Lett 2000;84:4184–7.
[3] Pendry JB. Negative refraction makes a perfect lens. Phys Rev Lett 2000;85:3966–9.
[4] Alù A, Engheta N. Plasmonic and metamaterial cloaking: physical mechanisms and potentials. J Opt A: Pure Appl Opt 2008;10:093002.
[5] Schurig D, Mock JJ, Justice BJ, Cummer SA, Pendry JB, Starr AF, et al. Metamaterial electromagnetic cloak at microwave frequencies. Science 2006;314:977–80.
[6] Seddon N, Bearpark T. Observation of the inverse Doppler effect. Science 2003;302:1537–40.
[7] Liu Z. Locally resonant sonic materials. Science 2000;289:1734–6.
[8] Pai PF. Metamaterial-based broadband elastic wave absorber. J Intell Mater Syst Struct 2010;21:517–28.
[9] Sun H, Du X, Pai PF. Theory of metamaterial beams for broadband vibration absorption. J Intell Mater Syst Struct 2010;21:1085–101.
[10] Pai PF, Peng H, Jiang S. Acoustic metamaterial beams based on multi-frequency vibration absorbers. Int J Mech Sci 2014;79:195–205.
[11] Bozorgnia Y, Bertero VV. Earthquake Engineering: From Engineering Seismology to Performance-Based Engineering. Taylor & Francis; 2004.

[12] Kim S-H, Das MP. Seismic waveguide of metamaterials. Mod Phys Lett B 2012;26:1250105.
[13] Jensen JS. Phononic band gaps and vibrations in one- and two-dimensional mass–spring structures. J Sound Vibrat 2003;266:1053–78.
[14] Martinsson PG, Movchan AB. Vibrations of lattice structures and phononic band gaps. Quart J Mech Appl Math 2003;56:45–64.
[15] Willis JR, Milton GW. On modifications of Newton's second law and linear continuum elastodynamics. Proc R Soc A: Math, Phys Eng Sci 2007;463:855–80.
[16] Yao S, Zhou X, Hu G. Experimental study on negative effective mass in a 1D mass-spring system. New J Phys 2008;10:043020.
[17] Sigalas MM, Economou EN. Elastic waves in plates with periodically placed inclusions. J Appl Phys 1994;75:2845.
[18] Vasseur JO, Deymier PA, Frantziskonis G, Hong G, Djafari-Rouhani B, Dobrzynski L. Experimental evidence for the existence of absolute acoustic band gaps in two-dimensional periodic composite media. J Phys: Condens Matter 1998;10:5051–6064.
[19] Cheng Y, Xu J, Liu X. One-dimensional structured ultrasonic metamaterials with simultaneously negative dynamic density and modulus. Phys Rev B 2008;77.
[20] Cheng Y, Xu JY, Liu XJ. Broad forbidden bands in parallel-coupled locally resonant ultrasonic metamaterials. Appl Phys Lett 2008;92:051913.
[21] Zhu R, Huang HH, Huang GL, Sun CT. Microstructure continuum modeling of an elastic metamaterial. Int J Eng Sci 2011;49:1477–85.
[22] Pai PF. Highly Flexible Structures: Modeling, Computation, And Experimentation. Virginia: American Institute of Aeronautics and Astronautics; 2007.
[23] Bianchi JP, Balmes E, Vermot Des Roches G, Bobillot A. Using modal damping for full model transient analysis. Application to Pantograph/Catenary Vibration. Leuven, Belgium: ISMA; 2010.